

# An entanglement-enhanced atomic gravimeter

Christophe Cassens<sup>1,\*</sup>, Bernd Meyer-Hoppe<sup>1</sup>, Ernst Rasel<sup>1</sup>, and Carsten Klempt<sup>1,2</sup>

<sup>1</sup>*Leibniz Universität Hannover, Institut für Quantenoptik, Welfengarten 1, D-30167 Hannover, Germany*

<sup>2</sup>*Deutsches Zentrum für Luft- und Raumfahrt e.V. (DLR),  
Institut für Satellitengeodäsie und Inertialsensorik, Callinstraße 30b, D-30167 Hannover, Germany*

(Dated: April 30, 2024)

Interferometers based on ultra-cold atoms enable an absolute measurement of inertial forces with unprecedented precision. However, their resolution is fundamentally restricted by quantum fluctuations. Improved resolutions with entangled or squeezed atoms were demonstrated in internal-state measurements for thermal and quantum-degenerate atoms and, recently, for momentum-state interferometers with laser-cooled atoms. Here, we present a gravimeter based on Bose-Einstein condensates with a sensitivity of  $-1.7_{-0.5}^{+0.4}$  dB beyond the standard quantum limit. Interferometry with Bose-Einstein condensates combined with delta-kick collimation minimizes atom loss in and improves scalability of the interferometer to very-long baseline atom interferometers.

Atom interferometers, in particular light-pulse interferometers, are employed for sensing gravitational fields, with applications for gravimetry [1], gradiometry [2–5], tests of general relativity [6–8] and the detection of gravitational waves [9–17]. The resolution of the gravity signal is ideally bounded by the standard quantum limit (SQL) that scales with the square root of the atom number. Increasing the flux of ultracold atoms is a challenge and moreover, quantum density fluctuations eventually limit the achievable resolution [18]. These limits can be overcome by operating the interferometers with squeezed atomic input states, where entanglement between the atoms enables a suppression of these fundamental signal fluctuations.

Squeezing-enhanced sensitivities were demonstrated in a wide variety of systems [19], but mainly in internal degrees of freedom that do not couple to inertial forces. Entanglement of momentum modes was generated with colliding atoms [20–22] and in our previous work using atomic Bose-Einstein condensates (BEC) [23]. Proof-of-principle demonstrations of spin-squeezed Mach-Zehnder interferometers are so far based on laser-cooled atoms [24, 25]. The retrieval of a gravitational signal was not yet reported and the squeezing concepts with optical cavities and use of non-condensed atoms prevent a straightforward application for high-precision atom interferometry with longer free-fall times and large momentum transfer. An operation with Bose-Einstein condensates is desirable [26, 27], as they fulfill the stringent requirements on expansion velocities and spatial-mode control that are set by many high-precision applications.

Here we report the application of squeezed states in rubidium Bose-Einstein condensates to measure the gravitational acceleration with a sensitivity beyond the SQL. Two-mode squeezing is generated by spin-changing collisions, and transferred to single-mode squeezing on the magnetic-field-insensitive clock transition. Microwave

and Raman-laser pulses are combined to form a gravity-sensitive atom interferometer. The input state with  $-5.4_{-0.5}^{+0.4}$  dB spin squeezing enables an interferometer operation with a sensitivity of  $-3.9_{-0.7}^{+0.6}$  dB below the experimentally recorded coherent-state reference and  $-1.7_{-0.5}^{+0.4}$  dB below the theoretical SQL. An alternating operation of two interferometer sequences with different interrogation times yields an absolute measurement of the gravitational acceleration. Our concept can be implemented in existing large-scale BEC-based atom interferometers with small integration efforts.

The experimental sequence is depicted in Fig. 1. It consists of an initial squeezing in the spin degree of freedom (a, b) followed by three microwave (mw) pulses that form a spin-echo sequence (c). During the sequence, four Raman-laser pulses form a Mach-Zehnder interferometer sensitive to gravity. We initially create spin-squeezed ensembles of  $6 \cdot 10^3$  <sup>87</sup>Rb atoms in a crossed-beam optical dipole trap by spin-changing collisions from  $|F, m\rangle = |1, 0\rangle$  to  $|1, \pm 1\rangle$  [28, 29]. The homogeneous magnetic field of 90  $\mu$ T is actively stabilized within  $\pm 7$  nT and oriented in parallel to the Earth’s gravitational field. Spin-changing collisions are activated for 50 ms by dressing the clock transition ( $|1, 0\rangle \leftrightarrow |2, 0\rangle$ ) with a blue-detuned mw field, thus populating the levels  $|1, \pm 1\rangle$  with a two-mode squeezed vacuum state (Fig. 1 (a) left). Directly after the dipole trap is turned off, all density-dependent interactions cease. After 1 ms of free fall, the dipole trap is turned on again for 350  $\mu$ s in order to slow down the expansion of the cloud [23, 30]. Up to this point, the spin-squeezed state is magnetic-field sensitive to first order. To transfer the squeezed vacuum in  $|1, \pm 1\rangle$  to a magnetically-insensitive clock state, the large amount of atoms in  $|1, 0\rangle$  is transferred to  $|2, 0\rangle$  by a mw  $\pi$ -pulse. Atoms in  $|1, \pm 1\rangle$  are transferred to  $|1, 0\rangle$  by a  $\sigma^-$ -polarized radio-frequency (rf)  $\pi$ -pulse (Fig. 1 (a) right) that leaves the atoms in F=2 unaffected [31]. This process creates a single-mode squeezed [32] vacuum state in level  $|1, 0\rangle$  from the two-mode-squeezed vacuum state in levels  $|1, \pm 1\rangle$  [33], containing approximately 1.1 atoms. The few remaining atoms in the levels  $|1, \pm 1\rangle$  do not contribute to the interferometer sequence. For the determi-

\* Author to whom correspondence should be addressed:  
cassens@iqo.uni-hannover.de

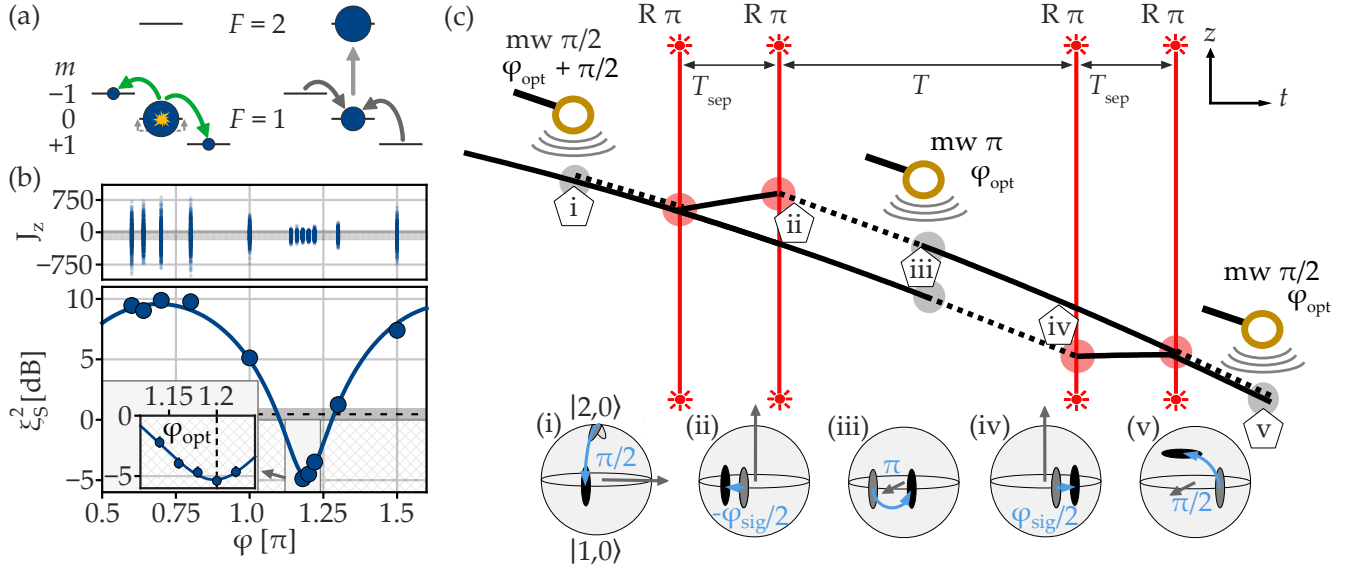


Fig. 1. The entanglement-enhanced gravimeter. (a) Generation of two-mode squeezing by spin-changing collisions (green) via microwave (mw) dressing, followed by a transfer to clock states via mw (light gray) and radio-frequency (rf) (dark gray) pulses. (b) Spin-noise tomography of the interferometer input state. The upper graph shows the normalized population in  $|2,0\rangle$  depending on the scanned mw phase  $\varphi$  with blue dots as individual measurements. In the bottom graph, the variance of these data points is compared to the SQL yielding a spin-squeezing parameter  $\xi_S^2$ . Error bars are smaller than the marker size. The inset shows a detailed measurement around the minimum that represents the optimal squeezing angle  $\varphi_{\text{opt}}$  (dashed line). The solid blue line presents a sinusoidal fit to the data, the dashed black line and gray area the experimental coherent state with  $0.5_{-0.4}^{+0.5}$  dB and the hatched area the spin-squeezed regime with sub-SQL fluctuations. (c) Interferometric sequence in a space-time diagram (top) and in Bloch-sphere representation (bottom). Dashed lines indicate the hyperfine level  $|1,0\rangle$  and solid lines  $|2,0\rangle$ . Hyperfine levels are changed by microwave (mw) and Raman pulses (R). Raman pulses also induce a state-dependent change in momentum mode. For the Bloch spheres, blue arrows indicate rotations and gray arrows the respective rotation axes. The north pole corresponds to  $|2,0\rangle$  and the south pole to  $|1,0\rangle$ . The squeezed input state is rotated into the phase-squeezed direction (i) and senses a phase  $\varphi_{\text{sig}}$  (ii-iv) that is finally mapped onto a population imbalance for readout (v).

nation of atom number distributions, we separate Zeeman levels with different  $m$  by a strong magnetic-field gradient and employ absorption detection.

We characterize the resulting spin-squeezed state in a spin-noise-tomography measurement [19]. The population imbalance

$$J_z = \frac{1}{2}(N_{F=2} - N_{F=1}) \quad (1)$$

is recorded after the spin-echo sequence with the mw pulses only. Fig. 1(b) shows fluctuations of  $J_z$  as a function of the global phase of the mw pulses. From the variance of the measured data at each phase, we obtain a spin squeezing parameter [19] of

$$\xi_S^2 = 4 \frac{\text{var}(J_z)}{N} \hat{=} -5.4_{-0.5}^{+0.4} \text{ dB} \quad (2)$$

at a mw phase of  $\varphi_{\text{opt}} = 1.2\pi$ . The corresponding anti-squeezing amounts to  $9.9_{-0.5}^{+0.4}$  dB at  $\varphi_{\text{opt}} + \frac{\pi}{2}$ . This spin-squeezed state is insensitive to magnetic field fluctuations to first order and subsequently employed to decrease the quantum noise in an inertially sensitive interferometer sequence.

The interferometric measurement (Fig. 1 (c)) starts by a mw  $\frac{\pi}{2}$ -pulse with a phase  $\varphi_{\text{opt}} + \frac{\pi}{2}$ . In this orientation,

the state features a minimal uncertainty of the phase between the two clock states (i). After 1.9 ms, a Raman  $\pi$ -pulse driving the transition  $|1,0;p=0\rangle \rightarrow |2,0;p=\hbar k_{\text{eff}}\rangle$  with 98.1(7) % efficiency [32] renders the interferometer sensitive to acceleration (ii). The Raman pulse transfers two-photon momenta  $\hbar k_{\text{eff}}$  and leads to a spatial delocalization of the two momentum modes. The  $\tau_R = 60 \mu\text{s}$  long Raman pulse is Blackman-shaped [34] to suppress the unwanted transition  $|2,0;p=0\hbar k\rangle$  to  $|1,0;p=-\hbar k_{\text{eff}}\rangle$ , which is only  $2\pi \times 30$  kHz detuned. The two clouds separate for  $T_{\text{sep}} = 77 \mu\text{s}$ , before a second Raman  $\pi$ -pulse decelerates the upper arm of the interferometer by driving the same transition. While the two clouds fall in the same momentum mode for a time  $T$ , the internal states are inverted by a resonant mw  $\pi$ -pulse to echo the spin evolution and suppress common noise like differential AC-Stark shifts, mw and Raman phase noise, and systematic mw frequency offsets (iii). After the inverting echo pulse, the two arms acquire an additional gravitational phase shift, now with opposite sign (iv), such that it is not canceled by the echo sequence. The clouds are reunited by performing the identical Raman processes on the lower arm of the interferometer. 1.9 ms after the mw  $\pi$ -pulse, the imprinted inertial phase with squeezed quantum noise is mapped onto the popu-

lation imbalance  $J_z$  by a microwave  $\frac{\pi}{2}$ -pulse with phase  $\varphi_{\text{opt}}$  (v). The time between the final Raman and the closing mw pulse allows additional parasitic interferometer paths, that arise from incomplete Raman transfers, to detach from the main paths.

The frequency difference of the Raman laser beams is switched between the pulses according to a frequency chirp-rate which is varied around the value  $\alpha = 9.8126 \text{ m/s}^2 \times k_{\text{eff}}$ . This frequency chirp counteracts the gravitational phase  $g \times k_{\text{eff}}$  perceived by the freely falling atoms, yielding a recorded phase signal of

$$\varphi_{\text{sig}} = \left( g - \frac{\alpha}{k_{\text{eff}}} \right) S(T, T_{\text{sep}}, \tau_R). \quad (3)$$

Here,  $g$  is the gravitational acceleration of the atoms and  $S$  is a scale factor depending on the interferometer geometry and the Raman pulse duration and shape [35].

If the chirp rate is set to exactly cancel the gravitational shift, the imprinted inertial phase vanishes according to Eq. 3 for all scaling factors. By choosing a phase difference of  $\frac{\pi}{2}$  between the opening and closing mw  $\frac{\pi}{2}$ -pulses, the accumulated phase maps to a measurement of  $J_z = 0$  (mid-fringe position). Fig. 2(a) shows the normalized population in  $F = 2$  for three different durations  $T$ . From the interception of the curves, an approximate value for the compensating chirp rate and a corresponding working range can be extracted.

The determination of the gravitational acceleration and the entanglement-enhanced sensitivity is performed by an alternating measurement of the normalized population in  $F = 2$  for two different durations  $T_1 = 455 \mu\text{s}$  and  $T_2 = 155 \mu\text{s}$  at the previously determined chirp-rate. This alternating operation suppresses the influence of drifts of the Raman pulse efficiencies that are slow with respect to the cycle time of 52 s. Since the scale factors and the corresponding slopes at this point differ, an experimental value for the gravitational acceleration  $g_{\text{exp}}$  can be obtained from the difference

$$\delta p = p(T_1) - p(T_2) = \frac{N_{F=2}(T_1)}{N(T_1)} - \frac{N_{F=2}(T_2)}{N(T_2)} \quad (4)$$

of the normalized populations of  $|F = 2\rangle$  (see Fig. 2 (a) inset) according to

$$g_{\text{exp}} = \frac{2}{C} \frac{\delta p}{S(T_1) - S(T_2)} + \frac{\alpha}{k_{\text{eff}}} \quad (5)$$

with contrast  $C = 98.0(1.4)\%$  obtained from the full fringes in Fig. 2(a) and respective scale factors  $S(T_1) = -1.42(1) \frac{\text{s}}{\text{m}^2}$  and  $S(T_2) = -0.767(3) \frac{\text{s}}{\text{m}^2}$ . The measured value of  $g_{\text{exp}} = 9.8118(16) \frac{\text{m}}{\text{s}^2}$  agrees with the local gravitational acceleration of  $9.812637196(88) \text{ m/s}^2$  [36] within the bounds of one standard error. Note that the error of the scale factors contributes much less to the uncertainty in  $g_{\text{exp}}$  than the statistical uncertainty. Furthermore, the scale factors inferred from the fringe measurements are reproduced by the theoretical calculation [32].

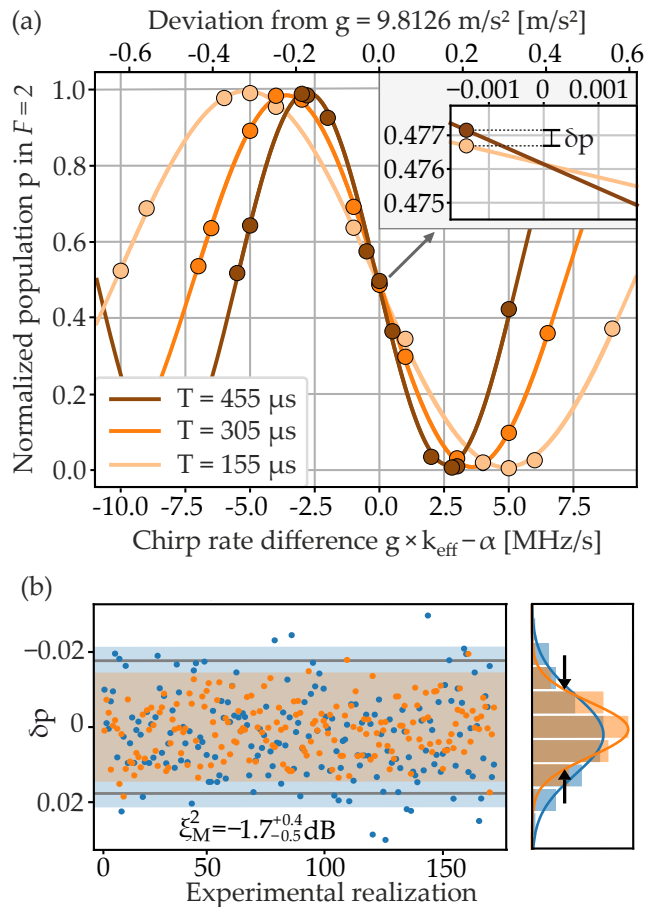


Fig. 2. Contrast and mid-fringe measurement. (a) Interferometer fringes for three different times  $T$  of the squeezed gravimeter depicted in Fig. 1(c) over chirp rate  $\alpha$ . From the sinusoidal fits, we infer a contrast of 98.0(1.4)%. All interferometer fringes intercept for the chirp rate which compensates the gravitational acceleration of the atoms in accordance with Eq. 3. The standard deviation of the measurements is smaller than the markers. The inset zooms into the crossing region from which the local gravitation  $g_{\text{exp}}$  is obtained by a measurement of the difference signal  $\delta p$ . (b) Gravimetry signal  $\delta p$  as interferometer output. The gravimeter signal of the squeezing-enhanced operation (orange) has reduced fluctuations compared to the operation with a coherent state (blue). Experimentally, we achieve a metrologically relevant reduction of the variance of  $-3.9_{-0.7}^{+0.6}$  dB compared to the experimentally recorded coherent input state and  $\xi_M^2 = -1.7_{-0.5}^{+0.4}$  dB compared to the theoretical SQL. Shaded areas indicate  $\pm 2$  standard deviations of the respective data, grey lines  $\pm 2$  standard deviations corresponding to the SQL.

We evaluate the metrological improvement by comparing the recorded measurement fluctuations with the optimal result from an ideal unentangled coherent state. We obtain a metrological squeezing factor

$$\xi_M^2 = \frac{4}{C^2} \frac{\text{Var}(J_z(T_1) - J_z(T_2))}{N(T_2) + N(T_1)} \hat{=} -1.7_{-0.5}^{+0.4} \text{ dB}, \quad (6)$$

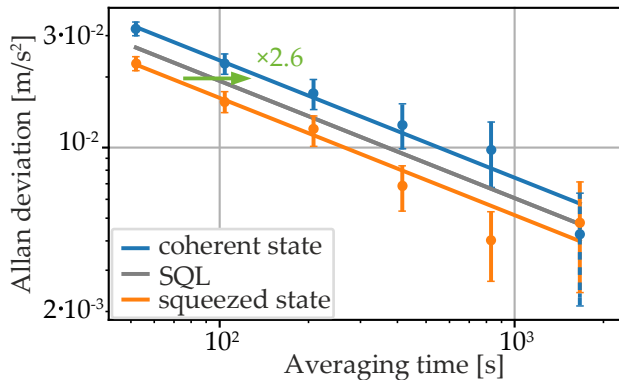


Fig. 3. Allan deviation of the gravimeter sequence using coherent states (blue) and squeezed states (orange). The squeezing-enhanced sequence reaches any instability 1.5-times faster than the theoretical optimum at the SQL (gray line) and 2.6-times faster than the experimentally recorded equivalent with coherent states. The technical noise sources for both sequences were the same.

where  $(N(T_2) + N(T_1))/4$  is the SQL of the difference of two independent measurements with their respective atom numbers  $N(T_2)$  and  $N(T_1)$ . This improvement proves the entanglement-enhanced measurement of the gravitational acceleration and constitutes the main result of our work. The corresponding data is shown in Fig. 2(b) in comparison to a coherent state realization.

We further analyze the temporal behavior throughout the measurement runs by calculating the Allan deviations [37] of  $\delta p$  for a coherent and a squeezed input state shown in Fig. 3. The coherent-state case is realized by omitting the squeezing generation section in the original experimental sequence. The squeezed-state results outperform the coherent-state equivalent over the whole range of averaging times. From a fit to the first 800 s of averaging time, we conclude that the squeezed-state signal averages down 2.6-times faster than the coherent-state signal and 1.7-times faster than the SQL for the same number of employed atoms.

In summary, we have presented a concept for enhancing atomic gravimeters beyond the SQL. Our demonstration involves all components for a large-scale implementation aiming for highest sensitivities. The squeezing method can be implemented in existing BEC-based atomic sources and can be scaled to large atom numbers due to the utilization of vacuum squeezing. The measured anti-squeezing is lower compared to other squeezing protocols like cavity-QND and helps to maintain a large contrast and dynamical range in the interferometry signal. The implementation with Bose-Einstein condensates provides low expansion velocities and exquisite control of the spatial mode to suppress systematic effects due to laser wavefront curvature and distortion or Coriolis force [38]. We have shown that the squeezing is compatible with a further delta-kick reduction of the expansion

velocity as required for long interrogation times. The squeezing angle can be freely adjusted and enables the anticipation and suppression of density-dependent quantum fluctuations [18].

The observed reduction of the squeezing due to the interferometer sequence stems solely from technical noise of the Raman laser system which constitutes an independent task for reaching highest sensitivities. Compared to conventional Mach-Zehnder interferometers, our concept features equal spin states during separation and recombination, suppressing the sensitivity to light shifts, microwave shifts and magnetic field noise.

Our method recommends itself for differential measurements, as performed in gradiometry, tests of the universality of free fall, or gravitational wave detection. In such configurations, technical noise, e.g. induced by vibrations, is common mode and cancels, enabling the exploitation of entanglement enhancement. We envision the application of entanglement-enhanced interferometry at much increased interrogation times, either in large-scale fountains like the Very-Long Baseline Atom Interferometer [39] or in microgravity environments like the Einstein Elevator [40]. The latter is currently pioneered by the INTENTAS project which aims at demonstrating an entanglement enhancement for future space-borne high-precision atom interferometers. Further applications include measurements of fundamental constants [41–43] as well as tests of classicalization [44].

## DATA AVAILABILITY

The data that support the findings of this study are available from the corresponding author upon reasonable request.

## ACKNOWLEDGMENTS

We thank Fabian Anders, Théo Sanchez, Dennis Schlippert, Christian Schubert, Polina Feldmann, Luis Santos, Jens Kruse, Naceur Gaaloul for inspiring discussions. We acknowledge financial support from the Deutsche Forschungsgemeinschaft (DFG, German Research Foundation) – Project-ID 274200144 – SFB 1227 DQ-mat within the projects A02 and B01 and under Germany’s Excellence Strategy – EXC-2123 QuantumFrontiers – 390837967. B.M.-H. acknowledges support from the Hannover School for Nanotechnology (HSN). We acknowledge funding by the SQUEIS project – grant No 499225223 – within the QuantERA II Programme.

## AUTHOR CONTRIBUTIONS

## COMPETING INTERESTS

The authors declare no competing interests.

- [1] J. M. McGuirk, M. J. Snadden, and M. A. Kasevich, “Large Area Light-Pulse Atom Interferometry,” *Phys. Rev. Lett.*, vol. 85, pp. 4498–4501, Nov. 2000.
- [2] P. Asenbaum, C. Overstreet, T. Kovachy, D. D. Brown, J. M. Hogan, and M. A. Kasevich, “Phase Shift in an Atom Interferometer due to Spacetime Curvature across its Wave Function,” *Phys. Rev. Lett.*, vol. 118, p. 183602, May 2017.
- [3] S.-w. Chiow, J. Williams, N. Yu, and H. Müller, “Gravity-gradient suppression in spaceborne atomic tests of the equivalence principle,” *Phys. Rev. A*, vol. 95, p. 021603, Feb. 2017.
- [4] G. W. Biedermann, X. Wu, L. Deslauriers, S. Roy, C. Mahadeswaraswamy, and M. A. Kasevich, “Testing gravity with cold-atom interferometers,” *Phys. Rev. A*, vol. 91, p. 033629, Mar. 2015.
- [5] J. M. McGuirk, G. T. Foster, J. B. Fixler, M. J. Snadden, and M. A. Kasevich, “Sensitive absolute-gravity gradiometry using atom interferometry,” *Phys. Rev. A*, vol. 65, p. 033608, Feb. 2002.
- [6] S. Dimopoulos, P. W. Graham, J. M. Hogan, and M. A. Kasevich, “Testing General Relativity with Atom Interferometry,” *Phys. Rev. Lett.*, vol. 98, p. 111102, Mar. 2007.
- [7] S. Dimopoulos, P. W. Graham, J. M. Hogan, and M. A. Kasevich, “General relativistic effects in atom interferometry,” *Phys. Rev. D*, vol. 78, p. 042003, Aug. 2008.
- [8] C. Ufrecht, F. Di Pumpo, A. Friedrich, A. Roura, C. Schubert, D. Schlippert, E. M. Rasel, W. P. Schleich, and E. Giese, “Atom-interferometric test of the universality of gravitational redshift and free fall,” *Phys. Rev. Res.*, vol. 2, p. 043240, Nov. 2020.
- [9] S. Abend, B. Allard, I. Alonso, J. Antoniadis, H. Araujo, G. Arduini, A. Arnold, T. Aßmann, N. Augst, L. Badurina, A. Balaz, H. Banks, M. Barone, M. Barsanti, A. Bassi, B. Battelier, C. Baynham, B. Quentin, A. Belic, A. Beniwal, J. Bernabeu, F. Bertinelli, A. Bertoldi, I. A. Biswas, D. Blas, P. Boegel, A. Bogojevic, J. Böhm, S. Böhrringer, K. Bongs, P. Bouyer, C. Brand, A. Brimis, O. Buchmueller, L. Cacciapuoti, S. Calatroni, B. Canuel, C. Caprini, A. Caramete, L. Caramete, M. Carlesso, J. Carlton, M. Casariego, V. Charmandaris, Y.-A. Chen, M. L. Chiofalo, A. Cimbri, J. Coleman, F. L. Constantini, C. Contaldi, Y. Cui, E. Da Ros, G. Davies, E. d. P. Rosendo, C. Deppner, A. Derevianko, C. de Rham, A. De Roeck, D. Derr, F. Di Pumpo, G. Djordjevic, B. Dobrich, P. Domokos, P. Dornan, M. Doser, G. Drougakis, J. Dunningham, A. Duspayev, S. Easo, J. Eby, M. Efremov, T. Ekelof, G. Elertas, J. Ellis, D. Evans, P. Fadeev, M. Fani, F. Fassi, M. Fattori, P. Fayet, D. Felea, J. Feng, A. Friedrich, E. Fuchs, N. Gaaloul, D. Gao, S. Gardner, B. Garraway, A. Gauguier, S. Gerlach, M. Gersemann, V. Gibson, E. Giese, G. F. Giudice, E. Glasbrenner, M. Gündogan, M. G. Haehnel, T. Hakulinen, K. Hammerer, E. T. Hammeli, T. Harte, L. Hawkins, A. Hees, J. Heise, V. Henderson, S. Herrmann, T. Hird, J. Hogan, B. Holst, M. Holynski, K. Hussain, G. Janson, P. Jeglič, F. Jelezko, M. Kagan, M. Kalliokoski, M. Kasevich, A. Kehagias, E. Kilian, S. Koley, B. Konrad, J. Kopp, G. Kornakov, T. Kovachy, M. Krutzik, M. Kumar, P. Kumar, C. Laemmerzahl, G. Landsberg, M. Langlois, B. Lanihan, S. Lellouch, B. Leone, C. L. P. Lafitte, M. Lewicki, B. Leykauf, A. Lezeik, L. Lombriser, L. López, E. L. Asamar, C. L. Monjaraz, G. Luciano, M. M. Mohammed, A. Maleknejad, K. Markus, J. Marteau, D. Massonet, A. Mazumdar, C. McCabe, M. Meister, J. Menu, G. Messineo, S. Micalizio, P. Millington, M. Milosevic, J. Mitchell, M. Montero, G. Morley, J. Müller, Ö. Müstecaplıođlu, W.-T. Ni, J. Noller, S. Odzak, D. Oi, Y. Omar, J. Pahl, S. Paling, S. Pandey, G. Pappas, V. Pareek, E. Pasatembou, E. Pelucchi, F. P. dos Santos, B. Piest, I. Pikovski, A. Pilaftsis, R. Plunkett, R. Poggiani, M. Prevedelli, J. Puputti, V. P. Veettil, J. Quenby, J. Rafelski, S. Rajendran, E. M. Rasel, H. R. Sfar, S. Reynaud, A. Richaud, T. Rodzinka, A. Roura, J. Rudolph, D. Sabulsky, M. Safronova, L. Santamaria, M. Schilling, V. Schkolnik, W. Schleich, D. Schlippert, U. Schneider, F. Schreck, C. Schubert, N. Schwesens, A. Semakin, O. Sergijenko, L. Shao, I. Shipsey, R. Singh, A. Smerzi, C. F. Sopena, A. Spallicci, P. Stefanescu, N. Stergioulas, J. Ströhle, C. Struckmann, S. Tentindo, H. Throssell, G. M. Tino, J. Tinsley, O. T. Mircea, K. Tkalcic, A. Tolley, V. Tornatore, A. Torres-Orjuela, P. Treutlein, A. Trombettoni, Y.-D. Tsai, C. Ufrecht, S. Ulmer, D. Valuch, V. Vaskonen, V. V. Aceves, N. Vitinov, C. Vogt, W. von Klitzing, A. Vukics, R. Walser, J. Wang, N. Warburton, A. Webber-Date, A. Wenzlawski, M. Werner, J. Williams, P. Windapssinger, P. Wolf, L. Wörner, A. Xuereb, M. Yahia, E. Z. Cruzeiro, M. Zarei, M. Zhan, L. Zhou, J. Zupan, and E. Zupanič, “Terrestrial Very-Long-Baseline Atom Interferometry: Workshop Summary,” Oct. 2023.
- [10] M. Abe, P. Adamson, M. Borcean, D. Bortoletto, K. Bridges, S. P. Carman, S. Chattopadhyay, J. Coleman, N. M. Curfman, K. DeRose, T. Deshpande, S. Dimopoulos, C. J. Foot, J. C. Frisch, B. E. Garber, S. Geer, V. Gibson, J. Glick, P. W. Graham, S. R. Hahn, R. Harnik, L. Hawkins, S. Hindley, J. M. Hogan, Y. Jiang, M. A. Kasevich, R. J. Kellett, M. Kiburg, T. Kovachy, J. D. Lykken, J. March-Russell, J. Mitchell, M. Murphy, M. Nantel, L. E. Nobrega, R. K. Plunkett, S. Rajendran, J. Rudolph, N. Sachdeva, M. Safdari, J. K. Santucci, A. G. Schwartzman, I. Shipsey, H. Swan, L. R. Valerio, A. Vasonis, Y. Wang, and T. Wilkason, “Matter-wave Atomic Gradiometer Interferometric Sensor (MAGIS-100),” *Quantum Sci. Technol.*, vol. 6, p. 044003, July 2021.
- [11] L. Badurina, E. Bentine, D. Blas, K. Bongs, D. Bortoletto, T. Bowcock, K. Bridges, W. Bowden, O. Buchmueller, C. Burrage, J. Coleman, G. Elertas, J. Ellis, C. Foot, V. Gibson, M. G. Haehnel, T. Harte, S. Hedges, R. Hobson, M. Holynski, T. Jones, M. Langlois, S. Lellouch, M. Lewicki, R. Maiolino, P. Majewski, S. Malik, J. March-Russell, C. McCabe, D. Newbold, B. Sauer, U. Schneider, I. Shipsey, Y. Singh, M. A. Uchida, T. Valenzuela, M. van der Grinten, V. Vaskonen, J. Vosseveld, D. Weatherill, and I. Wilmot, “AION: An atom interferometer observatory and network,” *J. Cosmol. Astropart. Phys.*, vol. 2020, p. 011, May 2020.
- [12] B. Canuel, S. Abend, P. Amaro-Seoane, F. Badaracco, Q. Beauvils, A. Bertoldi, K. Bongs, P. Bouyer, C. Brax-

- maier, W. Chaibi, N. Christensen, F. Fitzek, G. Flouris, N. Gaaloul, S. Gaffet, C. L. G. Alzar, R. Geiger, S. Guellati-Khelifa, K. Hammerer, J. Harms, J. Hinderer, M. Holynski, J. Junca, S. Katsanevas, C. Klempt, C. Kozanitis, M. Krutzik, A. Landragin, I. L. Roche, B. Leykauf, Y.-H. Lien, S. Loriani, S. Merlet, M. Merzougui, M. Nofrarias, P. Papadakos, F. P. dos Santos, A. Peters, D. Plexousakis, M. Prevedelli, E. M. Rasel, Y. Rogister, S. Rosat, A. Roura, D. O. Sabulsky, V. Schkolnik, D. Schlippert, C. Schubert, L. Sidorenkov, J.-N. Siemß, C. F. Sopaqueta, F. Sorrentino, C. Struckmann, G. M. Tino, G. Tsagkatakis, A. Viceré, W. von Klitzing, L. Woerner, and X. Zou, “ELGAR—a European Laboratory for Gravitation and Atom-interferometric Research,” *Class. Quantum Grav.*, vol. 37, p. 225017, Oct. 2020.
- [13] G. M. Tino, A. Bassi, G. Bianco, K. Bongs, P. Bouyer, L. Cacciapuoti, S. Capozziello, X. Chen, M. L. Chiofalo, A. Derevianko, W. Ertmer, N. Gaaloul, P. Gill, P. W. Graham, J. M. Hogan, L. Iess, M. A. Kasevich, H. Katori, C. Klempt, X. Lu, L.-S. Ma, H. Müller, N. R. Newbury, C. W. Oates, A. Peters, N. Poli, E. M. Rasel, G. Rosi, A. Roura, C. Salomon, S. Schiller, W. Schleich, D. Schlippert, F. Schreck, C. Schubert, F. Sorrentino, U. Sterr, J. W. Thomsen, G. Vallone, F. Vetrano, P. Villoresi, W. von Klitzing, D. Wilkowski, P. Wolf, J. Ye, N. Yu, and M. Zhan, “SAGE: A proposal for a space atomic gravity explorer,” *Eur. Phys. J. D*, vol. 73, p. 228, Nov. 2019.
- [14] B. Canuel, A. Bertoldi, L. Amand, E. Pozzo di Borgo, T. Chantrait, C. Danquigny, M. Dovalé Álvarez, B. Fang, A. Freise, R. Geiger, J. Gillot, S. Henry, J. Hinderer, D. Holleville, J. Junca, G. Lefèvre, M. Merzougui, N. Mielec, T. Monfret, S. Pelisson, M. Prevedelli, S. Reynaud, I. Riou, Y. Rogister, S. Rosat, E. Cormier, A. Landragin, W. Chaibi, S. Gaffet, and P. Bouyer, “Exploring gravity with the MIGA large scale atom interferometer,” *Sci Rep*, vol. 8, p. 14064, Sept. 2018.
- [15] J. M. Hogan and M. A. Kasevich, “Atom-interferometric gravitational-wave detection using heterodyne laser links,” *Phys. Rev. A*, vol. 94, p. 033632, Sept. 2016.
- [16] J. M. Hogan, D. M. S. Johnson, S. Dickerson, T. Kovachy, A. Sugarbaker, S.-w. Chiow, P. W. Graham, M. A. Kasevich, B. Saif, S. Rajendran, P. Bouyer, B. D. Seery, L. Feinberg, and R. Keski-Kuha, “An atomic gravitational wave interferometric sensor in low earth orbit (AGIS-LEO),” *Gen Relativ Gravit*, vol. 43, pp. 1953–2009, July 2011.
- [17] S. Dimopoulos, P. W. Graham, J. M. Hogan, M. A. Kasevich, and S. Rajendran, “Atomic gravitational wave interferometric sensor,” *Phys. Rev. D*, vol. 78, p. 122002, Dec. 2008.
- [18] P. Feldmann, F. Anders, A. Idel, C. Schubert, D. Schlippert, L. Santos, E. M. Rasel, and C. Klempt, “Optimal squeezing for high-precision atom interferometers,” Nov. 2023.
- [19] L. Pezzè, A. Smerzi, M. K. Oberthaler, R. Schmied, and P. Treutlein, “Quantum metrology with nonclassical states of atomic ensembles,” *Rev. Mod. Phys.*, vol. 90, p. 035005, Sept. 2018.
- [20] M. Bonneau, J. Ruaudel, R. Lopes, J.-C. Jaskula, A. Aspect, D. Boiron, and C. I. Westbrook, “Tunable source of correlated atom beams,” *Phys. Rev. A*, vol. 87, p. 061603, June 2013.
- [21] P. Dussarrat, M. Perrier, A. Imanaliev, R. Lopes, A. Aspect, M. Cheneau, D. Boiron, and C. I. Westbrook, “Two-Particle Four-Mode Interferometer for Atoms,” *Phys. Rev. Lett.*, vol. 119, p. 173202, Oct. 2017.
- [22] R. Bücker, J. Grond, B. T. Manz, Stephanie, T. Betz, C. Koller, U. Hohenester, T. Schumm, A. Perrin, and J. Schmiedmayer, “Twin-atom beams,” *Nature Physics*, vol. 7, pp. 608–611, Aug. 2011.
- [23] F. Anders, A. Idel, P. Feldmann, D. Bondarenko, S. Loriani, K. Lange, J. Peise, M. Gersemann, B. Meyer-Hoppe, S. Abend, N. Gaaloul, C. Schubert, D. Schlippert, L. Santos, E. Rasel, and C. Klempt, “Momentum Entanglement for Atom Interferometry,” *Phys. Rev. Lett.*, vol. 127, p. 140402, Sept. 2021.
- [24] B. K. Malia, Y. Wu, J. Martínez-Rincón, and M. A. Kasevich, “Distributed quantum sensing with mode-entangled spin-squeezed atomic states,” *Nature*, vol. 612, pp. 661–665, Dec. 2022.
- [25] G. P. Greve, C. Luo, B. Wu, and J. K. Thompson, “Entanglement-enhanced matter-wave interferometry in a high-finesse cavity,” *Nature*, vol. 610, pp. 472–477, Oct. 2022.
- [26] S. S. Szigeti, S. P. Nolan, J. D. Close, and S. A. Haine, “High-precision quantum-enhanced gravimetry with a bose-einstein condensate,” *Phys. Rev. Lett.*, vol. 125, p. 100402, Sep 2020.
- [27] R. Corgier, N. Gaaloul, A. Smerzi, and L. Pezzè, “Delta-kick squeezing,” *Phys. Rev. Lett.*, vol. 127, p. 183401, Oct 2021.
- [28] C. D. Hamley, C. S. Gerving, T. M. Hoang, E. M. Bookjans, and M. S. Chapman, “Spin-nematic squeezed vacuum in a quantum gas,” *Nature Phys*, vol. 8, pp. 305–308, Apr. 2012.
- [29] J. Peise, I. Kruse, K. Lange, B. Lücke, L. Pezzè, J. Arlt, W. Ertmer, K. Hammerer, L. Santos, A. Smerzi, and C. Klempt, “Satisfying the Einstein–Podolsky–Rosen criterion with massive particles,” *Nat Commun*, vol. 6, p. 8984, Nov. 2015.
- [30] H. Ammann and N. Christensen, “Delta Kick Cooling: A New Method for Cooling Atoms,” *Phys. Rev. Lett.*, vol. 78, pp. 2088–2091, Mar. 1997.
- [31] P. Kunkel, M. Prüfer, S. Lannig, R. Rosa-Medina, A. Bonnin, M. Gärtner, H. Strobel, and M. K. Oberthaler, “Simultaneous Readout of Noncommuting Collective Spin Observables beyond the Standard Quantum Limit,” *Phys. Rev. Lett.*, vol. 123, p. 063603, Aug. 2019.
- [32] See Supplemental Material for additional information on the experimental setup, especially the raman-laser-and rf-setup, a theoretical description of the prepared squeezed state and a theoretical determination of the scale factors, which contains refs. [23, 34, 35, 45].
- [33] I. Kruse, K. Lange, J. Peise, B. Lücke, L. Pezzè, J. Arlt, W. Ertmer, C. Lisdar, L. Santos, A. Smerzi, and C. Klempt, “Improvement of an Atomic Clock using Squeezed Vacuum,” *Phys. Rev. Lett.*, vol. 117, p. 143004, Sept. 2016.
- [34] B. Meyer-Hoppe, M. Baron, C. Cassens, F. Anders, A. Idel, J. Peise, and C. Klempt, “Dynamical low-noise microwave source for cold-atom experiments,” *Review of Scientific Instruments*, vol. 94, p. 074705, July 2023.
- [35] B. Fang, N. Mielec, D. Savoie, M. Altorio, A. Landragin, and R. Geiger, “Improving the phase response of an atom

interferometer by means of temporal pulse shaping,” *New J. Phys.*, vol. 20, p. 023020, Feb. 2018.

- [36] J. M. Hartwig, *Analyse eines atomaren Gravimeters hinsichtlich eines Quantentests des Äquivalenzprinzips*. PhD thesis, Hannover : Gottfried Wilhelm Leibniz Universität Hannover, 2013.
- [37] W. Riley and D. A. Howe, “Handbook of Frequency Stability Analysis,” *NIST*, July 2008.
- [38] A. Peters, K. Y. Chung, and S. Chu, “Measurement of gravitational acceleration by dropping atoms,” *Nature*, vol. 400, pp. 849–852, Aug. 1999.
- [39] A. Lezeik, D. Tell, K. Zipfel, V. Gupta, É. Wodey, E. Rasel, C. Schubert, and D. Schlippert, “Understanding the gravitational and magnetic environment of a very long baseline atom interferometer,” Sept. 2022.
- [40] C. Lotz, T. Froböse, A. Wanner, L. Overmeyer, and W. Ertmer, “Einstein-Elevator: A New Facility for Research from  $\mu$  to 5,” *Gravitational and Space Research*, vol. 5, pp. 11–27, Dec. 2017.
- [41] L. Morel, Z. Yao, P. Cladé, and S. Guellati-Khélifa, “Determination of the fine-structure constant with an accuracy of 81 parts per trillion,” *Nature*, vol. 588, pp. 61–65, Dec. 2020.
- [42] J. B. Fixler, G. T. Foster, J. M. McGuirk, and M. A. Kasevich, “Atom interferometer measurement of the newtonian constant of gravity,” *Science*, vol. 315, no. 5808, pp. 74–77, 2007.
- [43] G. Rosi, F. Sorrentino, L. Cacciapuoti, M. Prevedelli, and G. M. Tino, “Precision measurement of the newtonian gravitational constant using cold atoms,” *Nature*, vol. 510, pp. 518–521, July 2014.
- [44] B. Schriniski, P. Haslinger, J. Schmiedmayer, K. Hornberger, and S. Nimmrichter, “Testing collapse models with bose-einstein-condensate interferometry,” *Phys. Rev. A*, vol. 107, p. 043320, Apr 2023.
- [45] Y. Kawaguchi and M. Ueda, “Spinor Bose–Einstein condensates,” *Physics Reports*, vol. 520, pp. 253–381, Nov. 2012.

## SUPPLEMENTARY MATERIAL

### Experimental setup

The momentum mode of the BEC is changed via Raman transitions of two counter-propagating laser beams. The laser beams are generated by two external-cavity diode lasers. The primary laser is frequency-locked onto the cooling laser of our magneto-optical trap with an offset of  $-2$  GHz. The secondary laser is phase-locked to the primary at a dynamically changeable frequency difference of about 6.83 GHz. The spatial modes of each laser is cleaned by one meter of single-mode optical fibre. The intensities are individually stabilized using a photodiode after the fibre and an acousto-optical modulator (AOM) before the fibre. After the fibre, the two linearly polarized beams are coupled on a polarizing beam splitter. One output port leads to a high-bandwidth photodiode to generate the signal for the phase lock. The other port is coupled into a switching AOM which is controlled by a direct digital synthesizer of our mw system [34]. The detuning with respect to the cooling laser transition is reduced to  $-1.72$  GHz due to the added frequency from the AOMs. The beams are changed into counter-rotating circular polarization before entering the experimental chamber. After leaving the experimental chamber, the beams are again converted to perpendicular linear polarizations, such that the first laser can be extracted by a polarizing beam splitter. The second laser is retroreflected towards the incoming beam, changing its circular polarization handedness at the position of the atoms [23]. This leads to only one combination of beams driving Raman transitions since all other are suppressed by choice of polarization.

### Characterization of the Raman coupling

The presence of light fields shifts atomic energy levels inversely proportional to the detuning from the respective transition (AC Stark shift). In our setup the states  $|F = 2, m_F = 0\rangle$  and  $|F = 1, m_F = 0\rangle$  are shifted proportional to the intensity of the primary and secondary laser, respectively. Due to the employed interferometer sequence, common light shifts do not contribute to the interferometer’s phase. Moreover, the differential AC Stark shift component can be suppressed by adjusting the relative intensity between primary and secondary laser. The optimal intensity ratio is experimentally determined by reducing the light-shift-induced phase accumulation during a mw Ramsey sequence due to a Raman pulse with 1 MHz detuning. To avoid being on the wrong fringe we start with short pulse duration which is only increased once the mid-fringe point is reached.

The noise contribution to the gravimeter signal by the AC Stark shift is estimated from the increased variance of a mw Mach-Zehnder interferometer. To this end, a  $2\pi \times 1$  MHz detuned and  $60 \mu\text{s}$  Blackman-shaped Raman

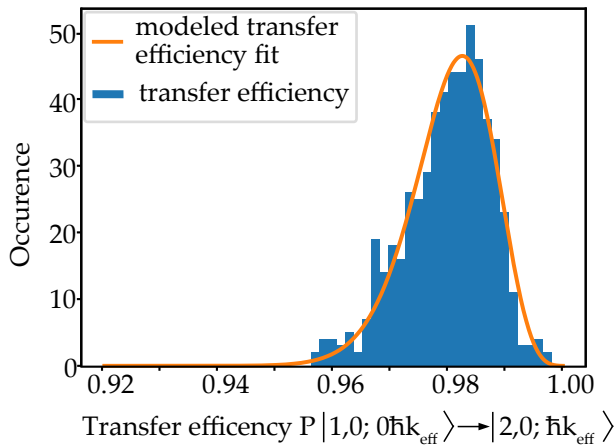


Fig. 4. Raman  $\pi$ -pulse efficiency. Transfer efficiency from  $|F = 1, m_F = 0; p = 0\rangle$  to  $|F = 2, m_F = 0; p = \hbar k\rangle$  of a  $64.8 \mu\text{s}$  Blackman-shaped Raman pulse. The mean transfer efficiency of 510 consecutive measurements is  $98.1(7)\%$ . Also shown is a fitted model of the transfer efficiency corresponding to an AC-Stark-shift induced detuning of  $2\pi \times 2.5 \text{ kHz}$  with fluctuations of  $2\pi \times 0.5 \text{ kHz}$ .

pulse is applied before and after the mw  $\pi$ -pulse in the mw interferometer sequence and the resulting noise level is compared to a sequence without Raman pulses. With light shift, the noise level is  $1.3_{-0.4}^{+0.4} \text{ dB}$  and without light shifts the interferometer signal features noise  $0.5_{-0.5}^{+0.4} \text{ dB}$  above the SQL. Considering the technical noise level due to intensity fluctuations from these measurements, one would expect a degradation of the spin squeezing due to light shifts to  $-2.6_{-1.9}^{+1.3} \text{ dB}$ . The AC Stark shift is thus the main noise source giving rise to the apparent reduction of the squeezing in the interferometer sequence.

For a  $\pi$  pulse, the transfer efficiency is measured to be  $98.1(7)\%$  (Fig. 4). In particular due to the chosen interferometer geometry, where parasitic paths are detached from the main path, this efficiency does not deteriorate the retrieved signal.

From weighted out-of-loop phase noise measurements we estimate a phase noise of  $\sigma_\phi = 1.2 \text{ mrad}$  for  $\tau_\pi = 25 \mu\text{s}$ ,  $T = 455 \mu\text{s}$  and  $T_{\text{sep}} = 50 \mu\text{s}$ . For the employed atom number of  $N = 6000$ , this corresponds to a noise contribution in  $J_z$  of  $\Delta J_z = 4$  or  $-20 \text{ dB}$  below the SQL. Phase noise is therefore a negligible noise contribution in our experiments.

## Single-mode squeezing

The Hamiltonian describing spin-changing collisions is given by [45]

$$\hat{H} = q \left( \hat{N}_{+1} + \hat{N}_{-1} \right) - \frac{\Omega}{N} \left[ \left( \hat{N}_0 - \frac{1}{2} \right) \left( \hat{N}_{+1} + \hat{N}_{-1} \right) + \hat{a}_0^\dagger \hat{a}_0 \hat{a}_{+1} \hat{a}_{-1} + \hat{a}_{+1}^\dagger \hat{a}_{-1}^\dagger \hat{a}_0 \hat{a}_0 \right] \quad (7)$$

with quadratic Zeeman energy  $q$ , spin interaction strength  $\Omega$  and the bosonic annihilation (creation) operators  $a_i^{(\dagger)}$  for level  $|1, i\rangle$ . Number operators are defined as  $\hat{N}_i = \hat{a}_i^\dagger \hat{a}_i$ . In the undepleted pump approximation,  $N_0 \approx N \gg 1$ , this results in

$$\hat{H} = (q - \Omega) \left( \hat{N}_{+1} + \hat{N}_{-1} \right) - \Omega \left( \hat{a}_{+1} \hat{a}_{-1} + \hat{a}_{+1}^\dagger \hat{a}_{-1}^\dagger \right). \quad (8)$$

When the quadratic Zeeman energy is now tuned to  $q = \Omega$  by microwave dressing, we are left with the two-mode squeezing Hamiltonian

$$\hat{H} = -\Omega \left( \hat{a}_{+1} \hat{a}_{-1} + \hat{a}_{+1}^\dagger \hat{a}_{-1}^\dagger \right) \quad (9)$$

that generates entangled pairs of atoms in the  $+1$  and  $-1$  levels. Introducing the symmetric and antisymmetric operators

$$\hat{a}_s = \frac{1}{\sqrt{2}} (\hat{a}_{+1} + \hat{a}_{-1}) \quad (10)$$

and

$$\hat{a}_a = \frac{1}{\sqrt{2}} (\hat{a}_{+1} - \hat{a}_{-1}), \quad (11)$$

we can rewrite the Hamiltonian as

$$\hat{H} = -\frac{\Omega}{2} (\hat{a}_s \hat{a}_s + \hat{a}_s^\dagger \hat{a}_s^\dagger) + \frac{\Omega}{2} (\hat{a}_a \hat{a}_a + \hat{a}_a^\dagger \hat{a}_a^\dagger) \quad (12)$$

$$= \hat{H}_s - \hat{H}_a. \quad (13)$$

This presents a combination of two single-mode squeezing operators for the symmetric ( $\hat{H}_s$ ) and the antisymmetric ( $\hat{H}_a$ ) superposition. By applying an rf pulse after the squeezing generation that only transfers the symmetric superposition from  $|1, \pm 1\rangle$ , we obtain a single-mode squeezed state in  $|1, 0\rangle$  (Fig. 1 a and b).

## Theoretical determination of the scale factor

In order to derive the local acceleration from the recorded normalized population in  $|2, 0\rangle$ , the scale factor  $S(T)$  (Eq. (3)) has to be determined.

The Blackman pulse shape [34] has to be taken into account [35],

$$\Omega_{\text{bm}}(t, t_0) = \Omega_0 \left( 0.42 - \frac{1}{2} \cos(2\pi\tilde{t}) + 0.08 \cos(4\pi\tilde{t}) \right),$$

where  $\Omega_0$  is the Rabi frequency corresponding to the maximal intensity and  $\hat{t} = t - t_0$  is the time passing since the beginning of the pulse  $t_0$ .

For the Blackman pulse shape, the sensitivity function  $g_{\text{bm}}(t)$  is given by

$$g_{\text{bm}}(t) = \sin \left( \int_{t_0}^t \Omega_{\text{bm}}(t', t_0) dt' \right).$$

The sensitivity function of the whole gravimeter sequence  $g_{\text{grav}}(t)$  is then given by

$$g_{\text{grav}}(t) = \begin{cases} g_{\text{bm}}(t, t_0), & t_0 < t < \tau_{\text{bm}}, \\ 1, & \tau_{\text{bm}} < t < \tau_{\text{bm}} + T_{\text{R}}, \\ 1 - g_{\text{bm}}(t, t_0 + \tau_{\text{bm}} + T_{\text{R}}), & \tau_{\text{bm}} + T_{\text{R}} < t < 2\tau_{\text{bm}} + T_{\text{R}}, \\ 0, & 2\tau_{\text{bm}} + T_{\text{R}} < t < 2\tau_{\text{bm}} + T_{\text{R}} + T, \\ -g_{\text{bm}}(t, t_0 + 2\tau_{\text{bm}} + T_{\text{R}} + T), & 2\tau_{\text{bm}} + T_{\text{R}} + T < t < 3\tau_{\text{bm}} + T_{\text{R}} + T, \\ -1, & 3\tau_{\text{bm}} + T_{\text{R}} + T < t < 3\tau_{\text{bm}} + 2T_{\text{R}} + T, \\ -1 + g_{\text{bm}}(t, t_0 + 3\tau_{\text{bm}} + 2T_{\text{R}}), & 3\tau_{\text{bm}} + 2T_{\text{R}} + T < t < 4\tau_{\text{bm}} + 2T_{\text{R}} + T, \\ 0, & \text{otherwise.} \end{cases}$$

The scale factor  $S(T)$  for given Blackman pulse duration  $\tau_{\text{bm}} = 60 \mu\text{s}$  and delocalization time  $T_{\text{R}} = 77 \mu\text{s}$  evaluates to

$$S(T) = k_{\text{eff}} \int_{t_0}^{4\tau_{\text{bm}} + 2T_{\text{R}} + T} g_{\text{grav}}(t_0, t) dt.$$

From this we get  $S(T = 455 \mu\text{s}) = 1.4290 \frac{\text{s}}{\text{m}^2}$  and

$S(T = 155 \mu\text{s}) = 0.7707 \frac{\text{s}}{\text{m}^2}$  which differs from the scale factors measured in Fig. 2(a) by only 0.7% and 0.5%.

For a small phase range around the mid-fringe position, the respective scale factors thus approximate the measured slopes  $\partial z / \partial g$  very well and the measured deviation remains small in comparison to the statistical fluctuations.